Solar Phys (2008) 250: 375–402
DOI 10.1007/s11207-008-9204-x

Stream Interactions and Interplanetary Coronal Mass Ejections at 5.3 AU near the Solar Ecliptic Plane

L.K. Jian · C.T. Russell · J.G. Luhmann · R.M. Skoug · J.T. Steinberg

Received: 20 January 2008 / Accepted: 7 May 2008 / Published online: 8 June 2008

Abstract We have performed a survey of the characteristics of two types of large spatial-scale solar-wind structures, stream interaction regions (SIRs), and interplanetary coronal mass ejections (ICMEs), near 5.3 AU, using solar-wind observations from *Ulysses*. Our study is confined to the three aphelion passes of *Ulysses*, and also within $\pm 10^{\circ}$ of the solar ecliptic plane, covering a part of 1992, 1997 – 1998, and 2003 – 2005, representing three slices of different phases of the solar activity cycle. Overall, there are 54 SIRs and 60 ICMEs in the survey. Many are merged in hybrid events, suggesting that they have undergone multiple interactions prior to reaching Jovian orbit. About 91% of SIRs occur with shocks, with 47% of such shocks being forward – reverse shock pairs. The solar-wind velocity sometimes stays constant or even decreases within the interaction region near 5.3 AU, in contrast with the gradual velocity increase during SIRs at 1 AU. Shocks are driven by 58% of ICMEs, with 94% of them being forward shocks. Some ICMEs seem to have multiple small flux

Electronic supplementary material The online version of this article (http://dx.doi.org/10.1007/s11207-008-9204-x) contains supplementary material, which is available to authorized users.

L.K. Jian (✉) · C.T. Russell
Institute of Geophysics and Planetary Physics, University of California Los Angeles, 595 Charles E. Young Dr. East, 6862 Slichter, Los Angeles, CA 90095, USA
e-mail: jlan@igpp.ucla.edu

C.T. Russell
e-mail: ctrussel@igpp.ucla.edu

J.G. Luhmann
Space Sciences Laboratory, University of California Berkeley, Berkeley, CA 94720, USA
e-mail: jgluhman@ssl.berkeley.edu

R.M. Skoug · J.T. Steinberg
Space Science and Applications, Los Alamos National Laboratory, Los Alamos, NM 87545, USA

R.M. Skoug
e-mail: rskoug@lanl.gov

J.T. Steinberg
e-mail: jsteinberg@lanl.gov

ropes with different scales and properties. We quantitatively compare various properties of SIRs and ICMEs at 5.3 AU, and study their statistical distributions and variations with solar activity. The width, maximum dynamic pressure, and peak perpendicular pressure of SIRs all become larger than ICMEs. Dynamic pressure ($P_{\rm dyn}$) is expected to be important for Jovian magnetospheric activity. We have examined the distributions of $P_{\rm dyn}$ of SIRs, ICMEs, and general solar wind, but these cannot explain the observed bimodal distribution of the location of the Jovian magnetopause. By comparing the properties of SIRs and ICMEs at 0.72, 1, and 5.3 AU, we find that the ICME expansion slows down significantly between 1 and 5.3 AU. Some transient and small streams in the inner heliosphere have merged into a single interaction region.

1. Introduction

In the solar wind, there are two main types of large-scale interactions: interactions between fast and slow streams and interactions between interplanetary coronal mass ejections (ICMEs) and the ambient solar wind. The former interaction, caused by a fast stream overtaking a preceding slow stream, can compress, deflect, and heat plasma, forming a stream interaction region (SIR). Magnetic forces help to determine the structure of SIRs (Gosling and Pizzo, 1999). With the solar rotation, the flow pattern associated with a SIR approximately corotates with the Sun and forms spirals in the solar equatorial plane, as illustrated in Figure 1. See Balogh *et al.* (1999) for a recent review.

About 24% of SIRs drive shocks at 1 AU (Jian *et al.*, 2006a). As the SIRs propagate outward, more and more bounding pressure waves steepen into shocks (*e.g.*, Hundhausen and Gosling, 1976; Smith and Wolfe, 1976). The stream interaction is centered around a stream interface (*e.g.*, Belcher and Davis, 1971; Burlaga, 1974; Gosling *et al.*, 1978; Schwenn, 1990), which is the plane separating the fast and slow streams. The compression and deflection of the flow occur through the forward and reverse pressure waves (shocks) that bound SIRs (*e.g.*, Crooker *et al.*, 1999).

SIRs can be recurrent structures commonly called corotating interaction regions (CIRs), associated with quasi-stable coronal source regions of the fast and slow streams (Belcher and Davis, 1971; Smith and Wolfe, 1976). They can also be transient events (Burlaga *et al.*, 1984), since coronal sources can change significantly on the time scale of one solar rotation (*e.g.*, Luhmann *et al.*, 2002, and references therein). In this study, we include CIRs in our SIR statistics and mark the long-lived CIRs separately in the survey.

ICMEs, as the interplanetary counterpart of coronal mass ejections (CMEs), often consist of several parts: a leading sheathlike pileup of solar-wind plasma and field sometimes preceded by a forward shock and a driver or ejecta portion, which is thought to represent new plasma and magnetic field injected from the corona into the heliosphere by the CME. ICMEs are commonly characterized by stronger than ambient magnetic field, rotating magnetic field, low β, leading forward shocks, declining velocity, low ion temperature, high density ratio of α particles to protons, bidirectional suprathermal electron (BDE) strahls, and unusual ion charge states (*e.g.*, Gosling *et al.*, 1991; Neugebauer and Goldstein, 1997; Gosling and Forsyth, 2001; Cane and Richardson, 2003; Russell and Shinde, 2005; Wimmer-Schweingruber *et al.*, 2006; Zurbuchen and Richardson, 2006). Many ICMEs do not exhibit all these signatures, and signatures are not always apparent. None of these features is unique to ICMEs or by itself constitutes a sufficient condition to identify an ICME (*e.g.*, Gosling, 1997; Neugebauer and Goldstein, 1997; Wimmer-Schweingruber *et al.*, 2006). So the identification of ICMEs is relatively subjective and is usually conducted based on several of these signatures.

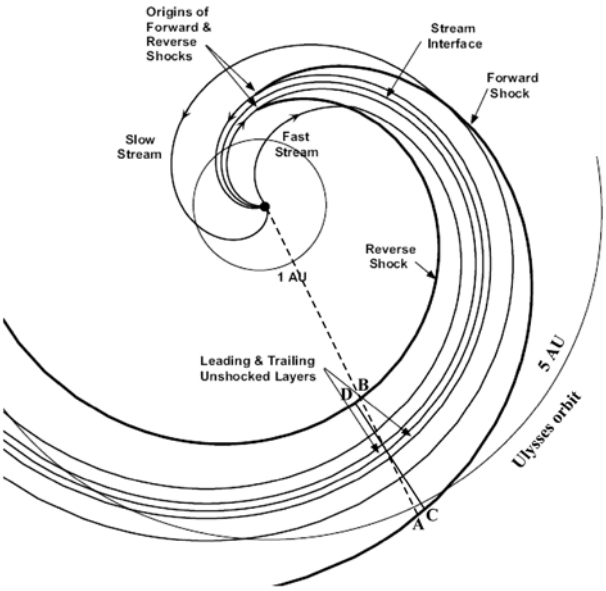

Figure 1 Schematic showing the expected IMF (interplanetary magnetic field) – SIR shock geometry when the ambient field consists of Parker spirals. Flow stream lines and magnetic field coincide in a frame of reference corotating with the Sun (after Intriligator *et al.*, 1995; Crooker *et al.*, 1999). Line AB is the radial extent of a SIR passing *Ulysses*, and line CD is the width perpendicular to the stream interface in the solar equatorial plane. Because of the tight Parker spiral at 5 AU, we can use the line AB to approximate the SIR width in this plane.

It is possible that ICMEs all contain a well-defined flux rope close to the Sun (Marubashi, 1997). As they evolve outward from the Sun, some flux-rope signatures may weaken (*e.g.*, Osherovich and Burlaga, 1997). In addition, some ICMEs may be encountered by the spacecraft far from the flux-rope axis where the flux-rope signatures are not clearly exhibited (*e.g.*, Borrini *et al.*, 1982; Jian *et al.*, 2005a; Riley *et al.*, 2006), since the angular widths of transient forward shocks can be larger than their drivers. In this scenario, only ICMEs penetrated by spacecraft at or close to the flux-rope axis exhibit low β and coherent internal magnetic-field rotations through a relatively large angle, and therefore can be identified as magnetic clouds (MCs) (*e.g.*, Burlaga *et al.*, 1981; Klein and Burlaga, 1982; Lepping, Jones, and Burlaga, 1990), which are usually treated as a specific subset of ICMEs.

SIRs and ICMEs, as well as their associated shocks, can affect the magnetic activity of planets. To fully understand the character of the heliosphere and provide space-weather forecasts, we need to understand the radial evolution of SIRs and ICMEs. We have performed comprehensive studies of SIRs and ICMEs using 10-year observations at both 0.72 and 1 AU (Jian *et al.*, 2006a, 2006b, 2008a) and studied their radial evolution from 0.72 to 1 AU (Jian *et al.*, 2008b). Here we extend our systematic study to an approximately fixed distance beyond 1 AU, with as long-term observations as possible.

The joint NASA/ESA *Ulysses* mission (Wenzel *et al.*, 1992) provides a good opportunity for such a study. Since its launch in October 1990, the *Ulysses* spacecraft has orbited the Sun two and a half times in a highly eccentric trajectory. The perihelion passes at 1.34 AU were relatively quick, taking only about 30 days to pass $\pm 10^\circ$ of the solar equatorial plane, whereas the aphelion passes took much longer. So far, *Ulysses* has passed aphelion at 5.41 AU three times – February 1992, April 1998, and June 2004 – acquiring 1004 days of observations within $\pm 10^\circ$ of the solar ecliptic plane. Since the *Ulysses* mission is likely to end sometime in 2008, these three passes are probably all the aphelion passes that will be made by *Ulysses*. We are interested in the region near the solar ecliptic plane, because most planets and spacecraft orbit near the ecliptic plane. In addition, since the data used for our solar-cycle studies at 0.72 and 1 AU were all obtained near the ecliptic plane, using *Ulysses*

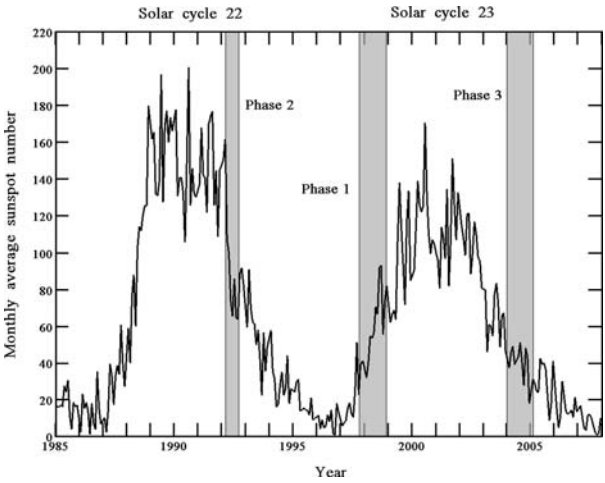

Figure 2 Monthly average sunspot number from 1985 to 2007 reported by US NOAA. The gray bars indicate the three periods used for this study. Based on the relative temporal sequence in a solar cycle, we order them into three phases, although different solar cycles may show some variability.

data also near the ecliptic plane would minimize the latitudinal variations from our inner heliosphere results and represent the radial variations better. To gather enough SIRs and ICMEs to be statistically representative, we chose a range of 10° rather than 7.25° (the inclination angle between solar ecliptic and equatorial planes). The three aphelion passes took place during different solar-activity phases. Considering the diverse distribution of these phases with respect to the solar cycle, shown in Figure 2, we use these observations to approximate the variation over the solar cycle.

Another benefit of this study is that we can characterize the space environment near Jupiter at different solar-cycle phases. The solar wind can exert a strong influence on the Jovian magnetosphere in changing its volume and shape, in energizing plasma, and in stimulating the aurora and a host of other associated effects (Southwood and Kivelson, 2001, and references therein). Hence, a quantitative description of solar-wind structures near Jovian orbit can also facilitate studies of Jovian magnetospheric phenomena.

Following the introduction of the *Ulysses* solar-wind data set in Section 2, we present our identification criteria for SIRs and ICMEs and show examples of SIRs, ICMEs, and hybrid events in Section 3. The solar-cycle variations and statistical distributions of the properties of SIRs and ICMEs are compared and discussed in Section 4. The radial evolution of SIRs and ICMEs obtained by comparing the observations at 0.72, 1, and 5.3 AU is addressed in Section 5.

2. *Ulysses* Solar Wind Data

As introduced in Section 1, this study focuses on the *Ulysses* aphelion passes within ±10° of the solar ecliptic plane. These three time periods are 1992, day 65 – day 261 (after the Jupiter fly-by); day 291 of 1997 – day 331 of 1998; and day 360 of 2003 – day 30 of 2005 (with no overlap with October – November 2003 superfast CMEs; *e.g.*, Gopalswamy *et al.*, 2006; de Kong *et al.*, 2005). They are respectively in the early declining phase of solar cycle 22, rising phase of solar cycle 23, and middle declining phase of solar cycle 23. Although there may be variations among different solar cycles, we put these three periods in the order 2, 1, and 3, following the temporal variation of a solar cycle, as given in Figure 2 and Table 1. These observations cover about 2.9° to – 17° in heliographic latitude and 5.26 – 5.41 AU in heliocentric distance. This study approximately represents the low-heliolatitude solar wind at a distance of 5.3 AU from the Sun.

We used 4-minute-resolution plasma data from the Solar Wind Observations Over the Poles of the Sun (SWOOPS) instrument (Bame *et al.*, 1992) and 1-second-resolution magnetic field data from the magnetometer (Balogh *et al.*, 1992) onboard the *Ulysses* spacecraft. The vector velocity and magnetic field shown in this paper are in heliospheric **RTN** coordinates, where **R** is the unit vector from the Sun to the spacecraft, **T** is $(\mathbf{\Omega} \times \mathbf{R})/|(\mathbf{\Omega} \times \mathbf{R})|$, where $\mathbf{\Omega}$ is the Sun's spin axis, and **N** completes the right-handed triad.

3. Criteria and Examples

We used the total perpendicular pressure (P_t) as a key parameter to study SIRs and ICMEs (*e.g.*, Jian *et al.*, 2005a, 2005b). It is the sum of the magnetic pressure and plasma thermal pressure perpendicular to the magnetic field, that is, $B^2/(2\mu_0) + \sum_j n_j \mathrm{k} T_{\mathrm{perp},j}$, where j represents the three major species in the solar wind: protons, electrons, and α particles. P_t is an important component in determining the evolution of magnetic structures in the solar wind (Russell, Shinde, and Jian, 2005). Because electron data were unavailable during late 2004 and 2005, we assumed a perpendicular electron temperature of 52 000 K during that interval. We used this value because it was the median $T_{\mathrm{perp,e}}$ from measurements in the available 2004 interval (before the electron data gap) and 1992 aphelion pass, which are both typical for the 2004 – 2005 period, and also because there should be little $T_{\mathrm{perp,e}}$ variation caused by the small heliocentric distance difference of the different periods.

Many interplanetary shocks were observed associated with large-scale interactions. The high-resolution magnetic field data help us to identify shocks; we also used plasma data to confirm the identifications. In addition, we have compared the shock lists from Balogh *et al.* (1995) and from Gosling and Forsyth (http://swoops.lanl.gov/shocks/). Sometimes, one event can drive multiple shocks. Consistent with our previous study at 1 AU, if one event occurred with multiple forward (or reverse) shocks without any reverse (or forward) shock, we count it as one event with only forward (or reverse) shock(s). If one event is associated with multiple forward (reverse) shocks and a reverse (forward) shock, we only count it as one event with a forward – reverse shock pair. In other words, all the events are counted at most once.

3.1. SIRs

The identification of SIRs was based on inspection of several features: an overall increase of solar-wind velocity V_p, a pileup of P_t with gradual decreases on both sides from the P_t peak to the edges of interaction region, V_p deflections, an increase of proton number density N_p, a compression of magnetic field **B**, an enhancement of proton temperature T_p, and an increase of the entropy defined as $\ln({T_p}^{3/2}/N_p)$ (Siscoe and Intriligator, 1993; Crooker *et al.*, 1996). Not all of these signatures are necessarily present in any one event, especially at 5.3 AU, where some solar-wind structures have merged. Therefore we require the presence of five signatures and also identify the SIRs with careful consideration of the ambient solar wind, such as nearby sector boundaries and ICMEs. Additionally, for ambiguous events, we checked the coronal source regions using the archive of synoptic maps from the Wilcox Solar Observatory magnetograph (Murdin, 2000).

The stream interface (SI) was identified by the P_t maximum within the interaction region, since force should be balanced at the interface. Its identification was also verified by a flow shear, an abrupt drop in N_p, an enhancement of T_p, and a high magnetic field intensity B in several events. But only a minority of SIRs had such a well-defined interface.

Table 1 Occurrence rates and shock association rates of SIRs and ICMEs.

Phase #	1		2		3		All	
Time interval	1997/291 – 1998/331		1992/65 – 261		2003/360 – 2005/30			
Solar cycle phase	Rising phase of solar cycle 23		Early declining phase of solar cycle 22		Declining phase of solar cycle 23		Various phases of the solar cycle	
No. of days	405		197		402		1004	
Category	SIR	ICME	SIR	ICME	SIR	ICME	SIR	ICME
Number of events (normalized annual number)	15 (14)	33 (30)	10 (19)	16 (30)	29 (26)	11 (10)	**54**	**60**
Number of events with hybrid events	10	11	6	8	3	3	19	22
% of events with hybrid events	66.7	33.3	60.0	50.0	10.3	27.3	**35.2**	**36.7**
% with shock(s)	93.3	57.6	100.0	56.3	86.2	63.6	**90.7**	**58.3**
% with only forward shock	53.3	54.5	20.0	56.3	34.5	54.5	37.0	55.0
% with only reverse shock	13.3	3.0	20.0	0.0	6.9	0.0	11.1	1.7
% with forward – reverse shock pair	26.7	0.0	60.0	0.0	44.8	9.1	42.6	1.7

Figures 3 and 4 display two SIRs observed at 5.4 AU in 2004. Their boundaries are easily identified from the obvious parameter changes. In the SI fixed reference frame, the P_t gradient arose to deflect the plasma that flowed toward the interface from both sides. In other words, the dynamic pressure P_{dyn} of the flow on both sides of the interface expressed in the SI reference frame was balanced by the P_t centered on the interface. Owing to the large magnitude and variations of N_p, the profile of P_{dyn} was dominated by N_p for both the SIRs and piled up for days, forming a plateau. The similarity of the N_p and P_{dyn} profiles was found in each of the examples shown in Figures 3 – 8. Compared with ambient solar wind, the suprathermal electron velocity distribution was enhanced within both the SIRs, especially in the fast streams.

In these two SIRs, the transitions of $V_p, \theta_V, \varphi_V, N_p$, and T_p across the SI (denoted by solid line *b*) were gradual, especially that of V_p. The selection of the SI was verified by an abrupt entropy increase following an entropy dip. West – East V_p deflections were observed in both SIRs, consistent with other studies (*e.g.*, Gosling and Pizzo, 1999, and references therein). The velocity deflection in the meridional (R – N) plane was unclear in Figure 3, perhaps because of a warped heliospheric current sheet (HCS). The meridional deflection within the SIR of Figure 4 was not simple either, being northward twice and then finally southward.

Rather than a gradual velocity increase as found in many SIRs at and within 1 AU, the V_p in Figure 3 decreased by 30 – 50 km s^{-1} between the leading and trailing edges of the SIR and then abruptly jumped more than 50 km s^{-1} at the reverse shock to reach a speed faster than the leading edge, resulting in an overall V_p enhancement for the SIR. Within the SIR shown in Figure 4, V_p stayed near 430 km s^{-1}, with speed changes mainly only at the leading discontinuity and the trailing reverse shock. (Note that shocks are marked as short-dashed lines in all these event examples.) Such velocity variations occurred in many SIRs in our survey. This is also why we emphasized the "overall increase of V_p" rather than the "monotonic increase of V_p" in our SIR criterion.

From the simplified SIR configuration illustrated in Figure 1, the interaction region at 5.3 AU is usually bounded by a pair of forward – reverse shocks and should include shocked slow stream, unshocked slow stream, interface, unshocked fast stream, and shocked fast stream. In Figures 3 and 4, it is hard to separate these different layers; in particular, the V_p was almost flat within the leading and trailing edges. It is likely that the compression waves associated with the interaction formed near the Sun have affected the plasma far from the interface. In addition, the P_t profiles of these two SIRs were not a simple pileup with gradual declining portions at the two sides, indicating the existence of some complex interactions.

There are still many temporal fluctuations and irregular characteristics in the interaction regions at 5.3 AU. These may be attributed to a few different factors. One possibility is that the solar-wind streams already have unstable properties before they interact (González-Esparza and Smith, 1997), since coronal hole boundaries can change rapidly. Another factor could be the collision of streams with obstacles or transient events such as ICMEs along their propagation from the Sun.

3.2. ICMEs

We identified ICMEs using a combination of ICME signatures: a P_t enhancement, bidirectional electron flux, a stronger than ambient **B**, a relatively quiet and smooth rotation in **B**, a declining V_p, a low T_p, and a high α to proton density ratio N_α/N_p (Jian *et al.*, 2006b). At least three of these features were required to identify an ICME. The edges of ICMEs were identified from a consensus of available features (*e.g.*, Wimmer-Schweingruber *et al.*,

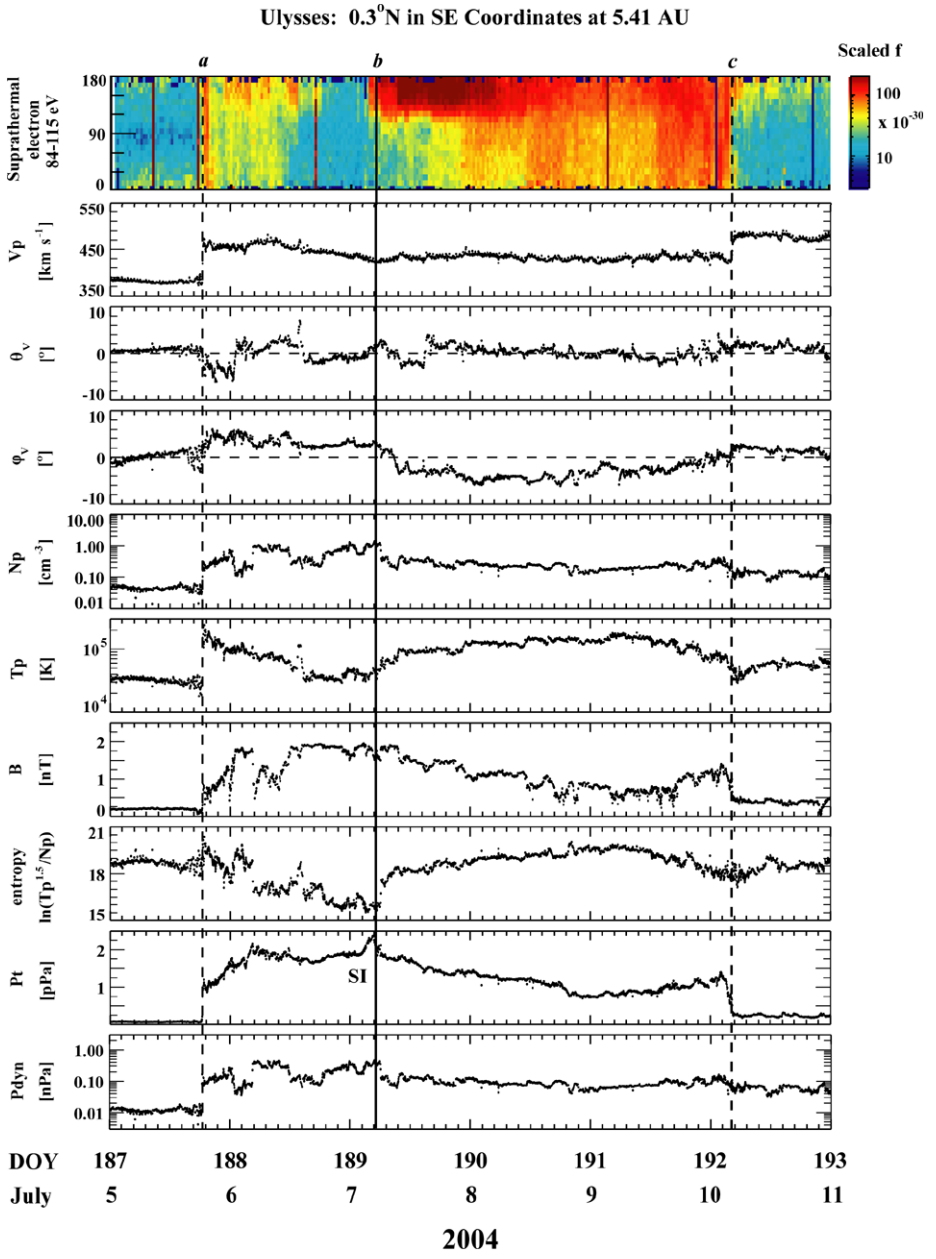

Figure 3 A SIR observed by *Ulysses* at 5.41 AU in 2004. *Ulysses* was at 0.3°N in solar ecliptic (SE) coordinates and about 6°S in heliographic (HG) coordinates. From top to bottom are pitch-angle distribution of the suprathermal electron (84 – 115 eV) velocity distribution ($s^3\ cm^{-6}$), scaled to 1 AU by multiplying by R^2, solar-wind proton speed (V_p), the meridional flow angle (θ_V) in the R – N plane with positive for flow to the north, the azimuthal flow angle (φ_V) in the R – T plane with positive for westward flow, proton density (N_p), proton temperature (T_p), magnetic field strength (B), entropy (S), total perpendicular pressure (P_t), and dynamic pressure (P_{dyn}). Dashed lines *a* and *c* mark the boundaries of the SIR, which were a pair of forward – reverse shocks; the solid line *b* denotes the stream interface (SI), where P_t peaked. In this case, N_p, T_p, and S all changed significantly at the interface. Shocks are indicated by short-dashed lines.

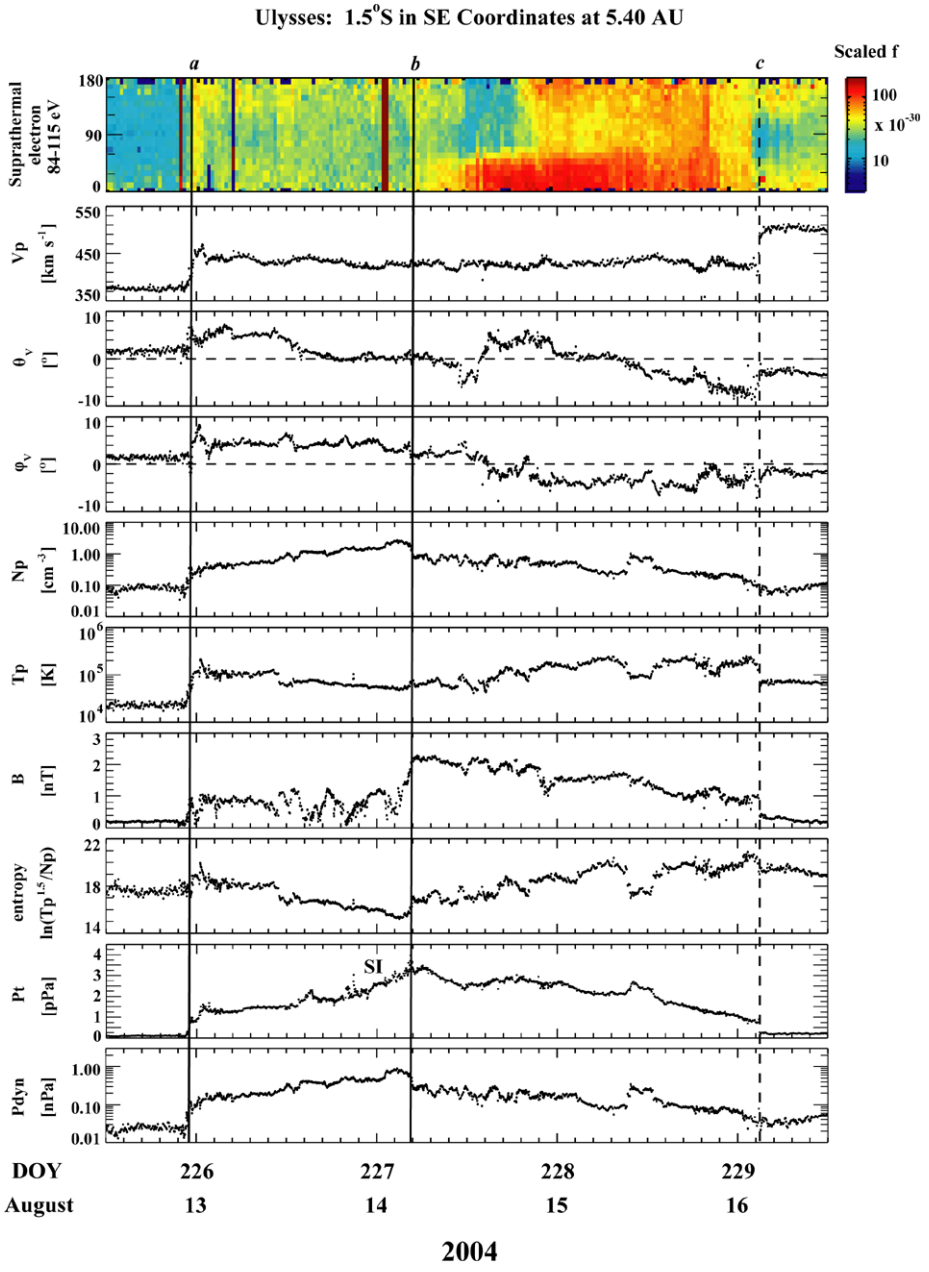

Figure 4 *Ulysses* observation of a SIR at 1.5°S in SE coordinates (about 8°S in HG coordinates) and at 5.40 AU in 2004, in the same format as Figure 3. Lines *a* and *c* mark the boundaries of the SIR, and the solid line *b* indicates the stream interface. There was a dissipation wave without a discontinuous increase in *B* at the solid line *a*, suggesting it probably had been a forward shock. A reverse shock is at dashed line *c*.

2006), usually delimited by sharp changes in plasma and magnetic field properties. For some ambiguous events, we checked the SOHO Large Angle and Spectrometric Coronagraph (LASCO) (Brueckner *et al.*, 1995) CME catalog (http://cdaw.gsfc.nasa.gov/CME_list/) to find the possible source CMEs and also referred to the ICME lists from Gosling and Reisefeld (http://swoops.lanl.gov/cme_list.html) and González-Esparza and Smith (1997), as well as the MC list from Crooker *et al.* (2004).

In our study of ICMEs at 0.72 and 1 AU, we found that the P_t temporal profiles of ICMEs could be roughly sorted into three characteristic patterns, which were associated with the observed MC signatures (Jian *et al.*, 2006b, 2008a). Corresponding to the Group 1, 2, and 3 ICMEs, the P_t profile, excluding any shock and/or sheath region (if present), respectively, has a central pressure maximum, a steady plateau, or a gradual decay. These patterns are consistent with a model in which each ICME has a central flux rope as proposed in Section 1, and the three groups of P_t profiles are due to different approach distances to the central flux rope. MCs, where the spacecraft observes a clear flux rope, most often are classified as Group 1 ICMEs (Jian *et al.*, 2006b). In contrast, Group 3 ICMEs rarely show a flux-rope geometry, consistent with an encounter in which flux-rope intersection is grazing or missing (*e.g.*, Borrini *et al.*, 1982). ICMEs with irregular P_t profiles were not assigned to a group.

The pressure P_t of the ICME in Figure 5 decayed sharply within 1 day (sheath region) after the leading shock, and then it remained lower than 0.5 pPa for 3.2 days (obstacle region) after 16 July, 0712 UT (Day of Year 198.3). With this irregular P_t profile, the event could not be classified into any of the ICME groups. In the obstacle region, N_p and β were relatively low, though with fluctuations; the BDE signature was prominent (first panel). Notably, the magnetic field was extremely quiet and the **B** rotations were quite coherent over 3 days in the obstacle. The P_t value was only about 25% of the P_t in the sheath region, suggesting strong compression in the sheath. However, the low P_t might be attributed to initial low plasma content when the CME erupted or to significant expansion of the flux rope during its transit to 5.3 AU.

The ICME in Figure 6 had the following signatures: declining V_p, high N_α/N_p, and relatively low β. BDE was observed for only part of the ICME, making this an example of ICMEs containing a mix of open, closed, and disconnected field lines (*e.g.*, Gosling, Birn, and Hesse, 1995; Shodhan *et al.*, 2000; Crooker *et al.*, 2004; Crooker and Horbury, 2006). P_t piled up in the leading part of the ICME. The ICME seemed to contain multiple flux ropes, as delimited by long-dashed lines $c-f$. These ropes differed in size and plasma properties, but the magnetic-field-intensity variations were relatively smooth across these ropes. There were several such ICMEs with multiple flux ropes in our survey. Because of the lack of a sheath-like region between the rotations, they are unlikely to be interacting CMEs (Rees and Forsyth, 2004). But they might result from the deformation of a CME in a Parker spiral-like fashion (*e.g.*, Rees and Forsyth, 2004, and references therein) or from flux ropes formed by magnetic reconnection in the solar wind (*e.g.*, Crooker, Gosling, and Kahler, 2002, and references therein). Vasquez *et al.* (2001) extensively studied the nature of fluctuations on directional discontinuities inside an ICME containing a sequence of ejecta material, during 23 – 26 December in 1996 at 1 AU. A similar close examination can be conducted for our events at 5.3 AU in the future.

3.3. Hybrid Events

During transit to 5.3 AU, SIRs and ICMEs have time for significant interaction and merging (*e.g.*, Burlaga, 1983; González-Esparza *et al.*, 1996; Whang *et al.*, 2001; Du,

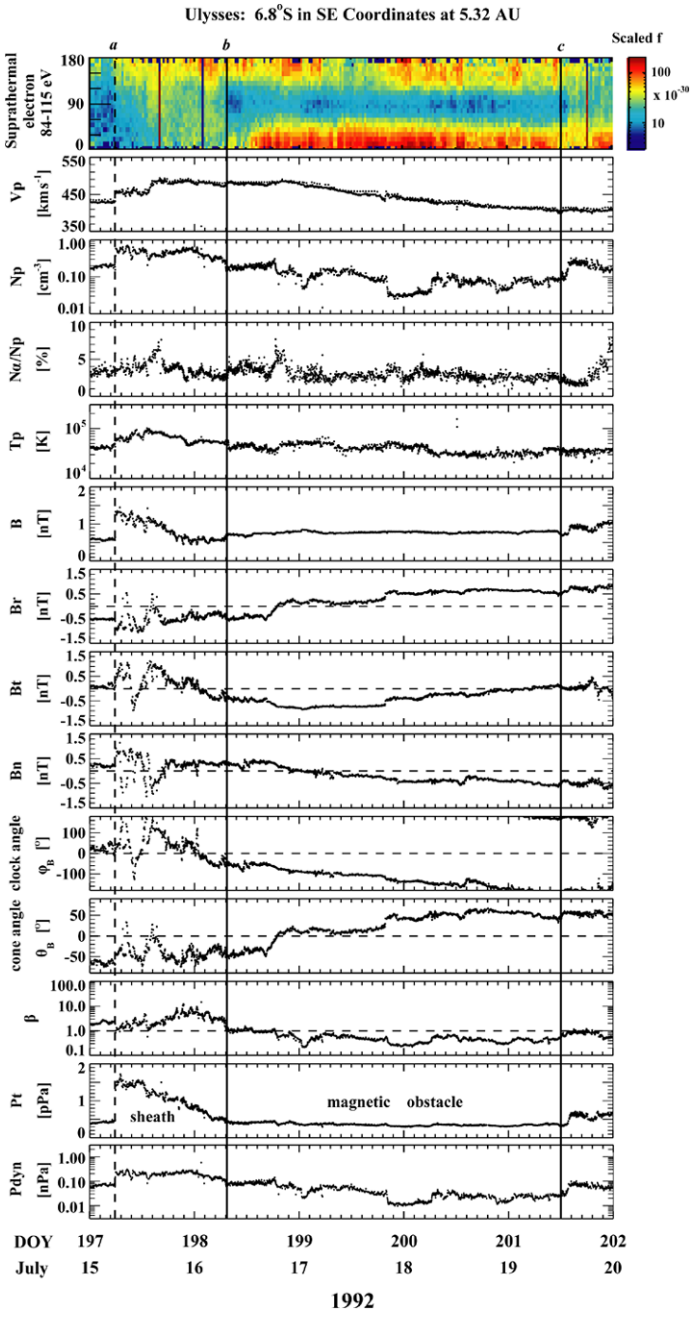

Figure 5 *Ulysses* observation of an ICME at 6.8°S in SE coordinates (about 8°S in HG coordinates) and at 5.32 AU in 1992. From top to bottom are pitch-angle distribution of the suprathermal electron (84 – 115 eV) velocity distribution ($s^3\ cm^{-6}$), scaled to 1 AU by multiplying by R^2, V_p, N_p, α to proton density ratio (N_α/N_p), T_p, B, magnetic field components in RTN coordinates, clock angle $(\arctan(B_t/B_n))$, cone angle $(\arcsin(B_r/B))$, β, P_t, and P_{dyn}. The sheath is the region between the lines a and b; a magnetic obstacle is the region between lines b and c. Bidirectional suprathermal electrons (BDEs) were prominent while P_t was very weak in the obstacle region. A forward shock is indicated by the short-dashed line a.

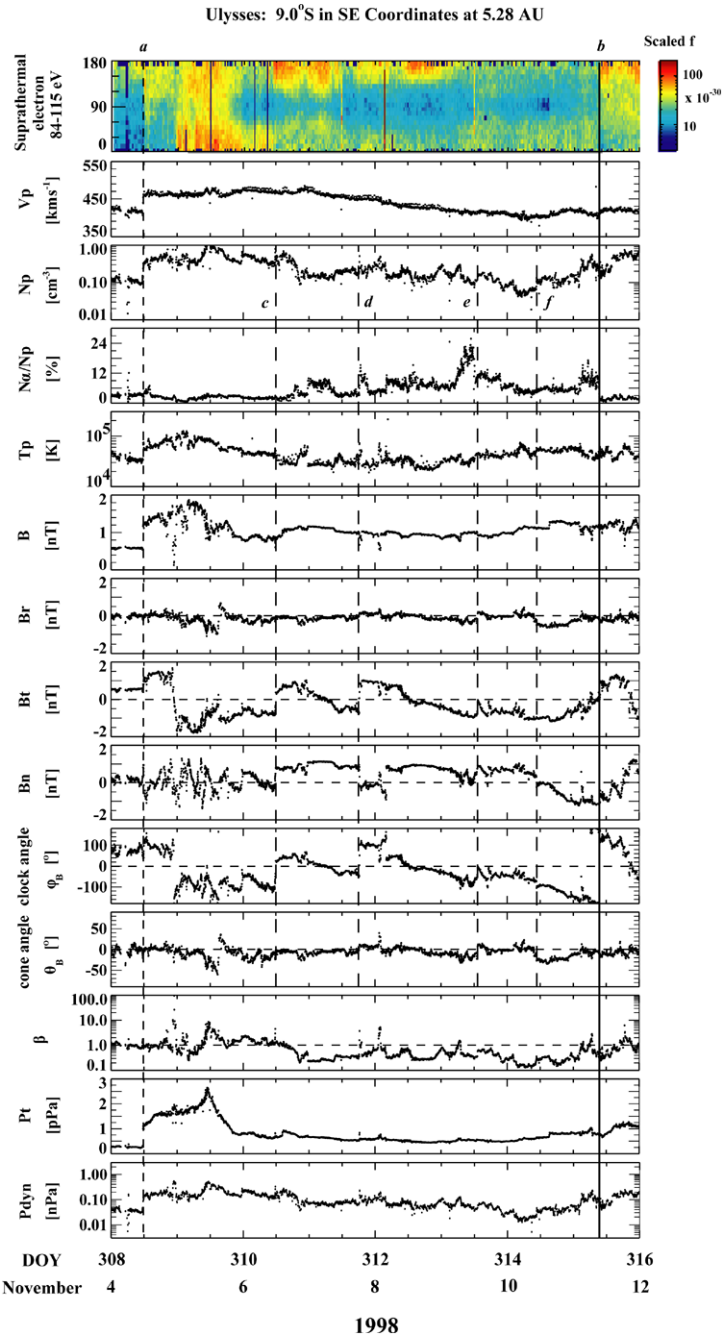

Figure 6 An ICME at 9.0°S in SE coordinates (16°S in HG coordinates) and at 5.28 AU in 1998, in the same format as Figure 5. A leading forward shock is at short-dashed line a. The enhanced and bidirectional suprathermal electron distribution is demonstrated in the first panel. Long-dashed lines $c - f$ separate multiple flux ropes, which had different sizes, field strengths, and plasma properties.

Wang, and Hu, 2007). Moreover, they could be deformed significantly in the Parker spiral topology. We found many events with irregular characteristics in our survey, and a number of them consisted of more than one event (*e.g.,* Burlaga *et al.*, 1981; Crooker, 2000). If the SIRs or ICMEs in such hybrid events were still representative, they were included in the SIR or ICME lists as appropriate and are marked by asterisks.

Figure 7 displays a good example of a hybrid event. It occurred during 12 September 0126 UT – 15 September 1033 UT (DOY 256.06 – 259.44) in 1992, where an ICME merged with a SIR. The ICME was characterized by relatively low $N_{\rm p}$ and $T_{\rm p}$, small β, high $N_\alpha/N_{\rm p}$, and quiet and strong B. It survived for about 6 hours (DOY 257.84 – 258.08) and added some complexity to the basic SIR morphology. Besides a pair of forward – reverse shocks bounding the SIR, a second forward shock was formed on 13 September 1355 UT (DOY 257.58), probably driven by the ICME. Over the 3.4-day SIR, the suprathermal electron flux was remarkably high, and the velocity $V_{\rm p}$ increased by more than 300 km s^{-1} in two steps, not monotonically. $V_{\rm p}$ had clear North – South and West – East deflections, which were quite smooth over the whole SIR. Rather than a gradual pileup as in a classic SIR, $P_{\rm t}$ increased by more than 10 pPa at the second shock and reached 23.5 pPa after that, one of the highest $P_{\rm tmax}$ values in our survey. However, $P_{\rm dyn}$ was not particularly high during this event, with a maximum of 1.2 nPa.

Figure 8 shows another hybrid event in 2004, with a SIR (24 November 1214 UT – 30 November 0523 UT, *i.e.*, DOY 329.510 – 335.224) containing a probable ICME (26 November 0600 UT – 27 November 1312 UT, *i.e.*, DOY 331.25 – 332.55). The solar wind speed was slow during the entire period. $V_{\rm p}$ increased from 345 to 440 km s^{-1} in steps through the SIR. There was a pair of forward – reverse shocks (short-dashed lines *b* and *c*), respectively, at 26 November 0600 UT (DOY 331.25) and 27 November 1312 UT (DOY 332.55). Within the region bounded by the shock pair, the $P_{\rm t}$ and $P_{\rm dyn}$ profiles showed a trough in the center, following the $N_{\rm p}$ and B profiles; $V_{\rm p}$ was apparently deflected; β decreased moderately; $T_{\rm p}$, $N_\alpha/N_{\rm p}$, and B were high; the clock and cone angles were nearly constant. The 1.3-day interval might be the relic of an ICME overtaken by a SIR, and the unusual $P_{\rm t}$ profile might be caused by the complicated interaction of a SIR and the ICME. Such concave-shape structures bounded by a pair of forward – reverse shock have been extensively discussed in Riley and Gosling (2007), Manchester and Zurbuchen (2007), and references therein. This event could provide a good example for tests of MHD solar-wind models at mid-heliocentric distances (about 5 AU), if the coronal sources can be identified.

3.4. SIR and ICME Surveys

In Appendices I and II (see the online supplementary material), we report comprehensive surveys of SIRs and ICMEs observed by *Ulysses* during its three aphelion passes. CIRs and hybrid events are marked in the surveys. Tabulated are the start and end times, associated shocks, $P_{\rm t}$ change at shocks, maximum of $P_{\rm t}(P_{\rm tmax})$, maximum of $P_{\rm dyn}(P_{\rm dynmax})$, maximum and minimum solar-wind velocity ($V_{\rm max}$ and $V_{\rm min}$) within each event (including the start and end points), maximum field intensity ($B_{\rm max}$), maximum and minimum proton temperature ($T_{\rm min}$ and $T_{\rm max}$), and group of ICMEs. Such surveys can also help the event study of Jovian magnetospheric phenomena (*e.g.*, Ge, Jian, and Russell, 2007).

In addition, we measured the maximum velocity change with time over one event (ΔV). Since overall the velocity increases across a SIR, ΔV is $V_{\rm max} - V_{\rm min}$, indicating the velocity variation from slow to fast stream within the SIR including the edges. The definition of ΔV

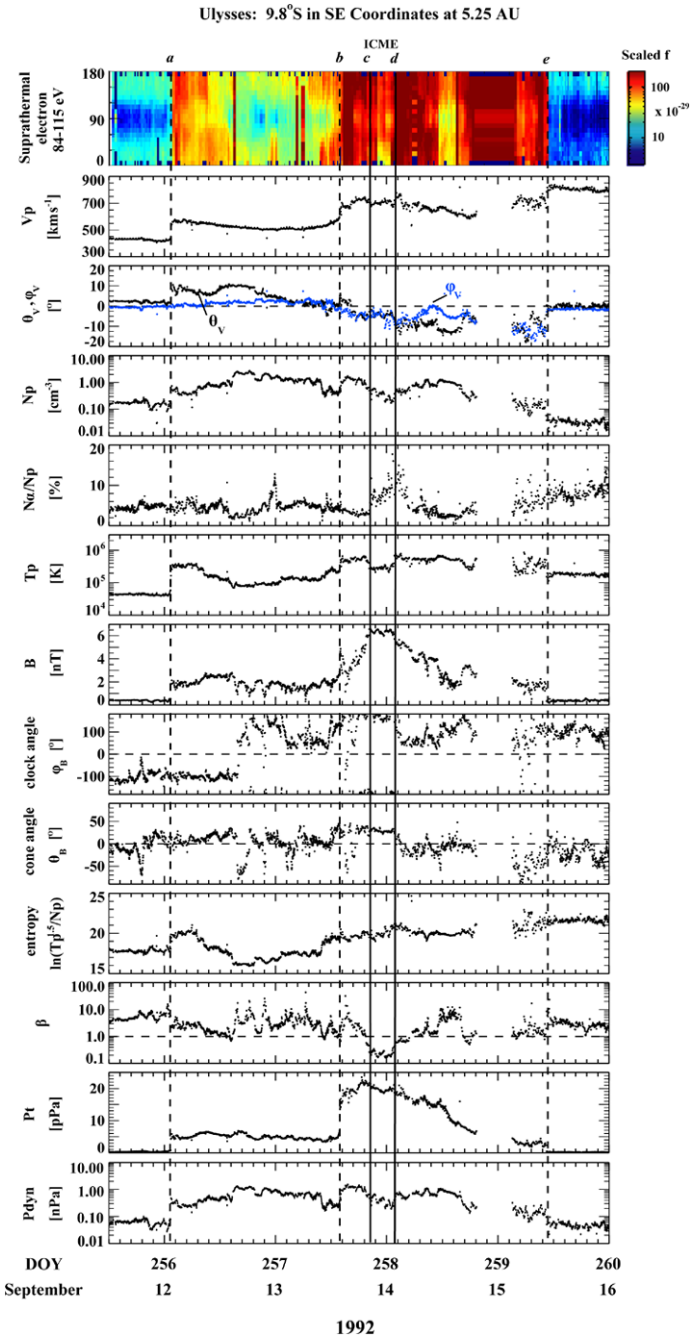

Figure 7 A SIR including a 0.3-day ICME at 9.8°S in SE coordinates (about 17°S in HG coordinates) and at 5.25 AU in 1992. From top to bottom are suprathermal electron velocity distribution, $V_{\rm p}$, meridional ($\theta_{\rm V}$, dark dots) and azimuthal ($\varphi_{\rm V}$, blue dots) flow angles, $N_{\rm p}$, α to proton density ratio, $T_{\rm p}$, B, clock angle, cone angle, entropy, β, $P_{\rm t}$, and $P_{\rm dyn}$. Dashed lines a and e indicate a pair of forward–reverse shocks, bounding the SIR. The dashed line b marks a forward shock, where $P_{\rm t}$ increased greatly. Solid lines c and d bound an ICME. The electron flux was very high, as shown in the first panel.

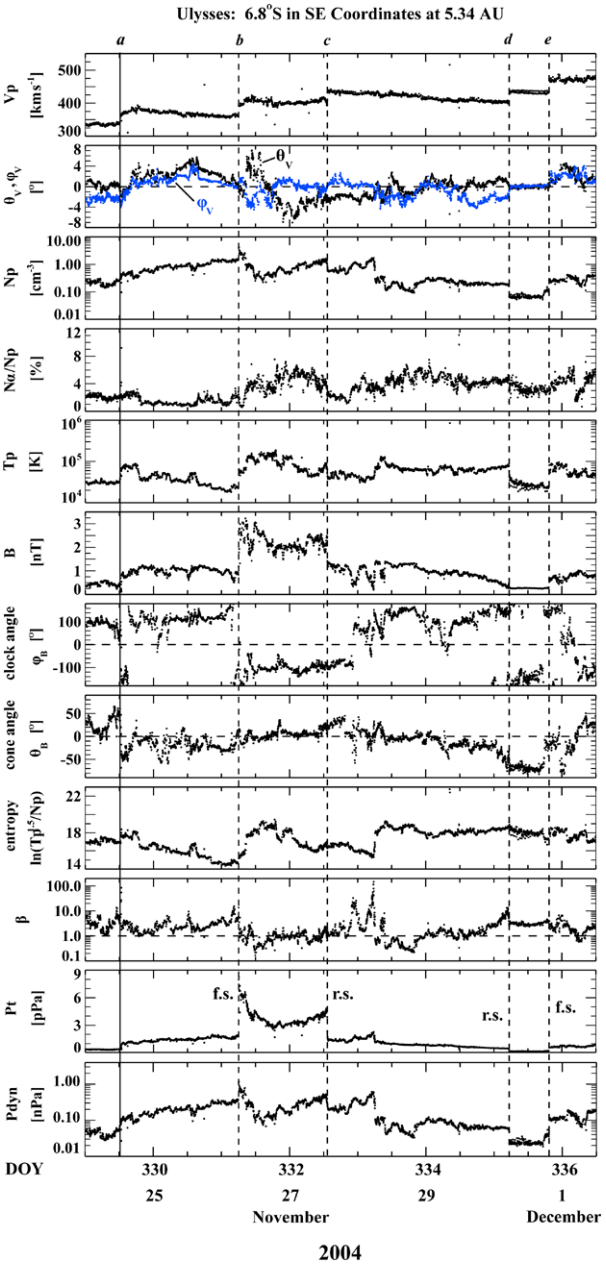

Figure 8 A SIR containing a possible 1.3-day ICME at 6.8°S in SE coordinates (14°S in HG coordinates) and at 5.34 AU in 2004, in the same format as Figure 7, except that the suprathermal electron data were unavailable during this time. Again, shocks are marked by short-dashed lines.

also applies to ICMEs. In our survey, 53 of 60 ICMEs (88.3%) have negative ΔV, indicating velocity decreasing with time in the ICMEs. Besides the possible effects of solar imprint, such a velocity decrease suggests that most ICMEs are still expanding at 5.3 AU. In the following, we only consider the absolute value of the velocity change ($|\Delta V|$) for ICMEs, which is also defined as the expansion velocity of ICMEs (*e.g.*, Jian *et al.*, 2008b). In any case, $|\Delta V|$ for both SIRs and ICMEs is given by $V_{\max} - V_{\min}$.

4. Properties of SIRs and ICMEs

In this section we discuss the properties of the SIRs and ICMEs in our survey, as presented in Tables 1 – 3 and Figures 9 – 11. As discussed in the introduction, we will use the variation over these three phases as an approximation of a whole solar cycle. Table 1 lists the occurrence rates, association rates with hybrid events, and shock association rates of SIRs and ICMEs at 5.3 AU. Tables 2 and 3, respectively, give statistics of the properties of the 54 SIRs and 60 ICMEs during each phase. The average, median, maximum, and minimum values of each parameter are given in the bottom four lines.

Figure 9 compares the approximate solar-cycle variations of the following properties of SIRs and ICMEs in the order of phase 1 to 3: normalized annual number of events, duration, width, P_{dynmax}, P_{tmax}, B_{max}, V_{mean} (estimated by the mean of V_{min} and V_{max}), and $|\Delta V|$. The bars indicate the corresponding probable errors of the mean. The y-axis scales for each parameter are the same for SIRs and ICMEs. The exact values are listed in Tables 2 and 3. To summarize the properties of the solar-wind environment around Jovian orbit, histograms of these properties are displayed in Figure 10. To visualize the diverse properties of SIRs and ICMEs, and to determine the correlations between different properties, we also show scatter plots of duration and width versus the V_{mean} of SIRs and ICMEs in Figure 11, where the radius of the circle for each event is proportional to P_{tmax}, and the color indicates P_{dynmax}.

At 5.3 AU, 74.1% of SIRs are CIRs, larger than the fraction at 0.72 and 1 AU (Jian *et al.*, 2008b). Considering the high fraction of CIRs, we do not separately address CIR solar-cycle variations and statistics here. We extensively describe and discuss the properties of SIRs and ICMEs in the Sections 4.1 to 4.6.

4.1. Occurrence Rates of Events and Associated Shocks

The three phases included observations from different numbers of days. We normalized the observed number of events by the fraction of available data during each phase to get an annual number of events, given in parentheses in Table 1. Overall, we observed 54 SIRs. The normalized annual occurrence rates were 20 for SIRs and 14 for CIRs, both smaller than in the inner heliosphere (Jian *et al.*, 2008b). The discrepancy may be related to the existence of more transient stream interactions in the inner heliosphere or to the merging of small streams as the SIRs evolve (*e.g.*, Burlaga, 1983; Whang *et al.*, 2001). Displayed in Figure 9(a), from phase 1 to 3, the normalized annual SIR number increased from 14 to 26, while the normalized annual CIR number varied more substantially, from 6 to 24 (not shown). The occurrence rates of SIRs and CIRs were both much higher in phase 3, during the middle of the declining phase of solar cycle 23. Such a solar-cycle variation is larger than that in the inner heliosphere (Jian *et al.*, 2008b). However, the relatively short term observations at 5.3 AU might cause some uncertainty in the statistics.

Shown in Table 1 and Figure 9(a), the normalized annual number of ICMEs varied nearly in phase with the solar activity, from 30 to 10. Such variation is similar to that observed in the inner heliosphere (Jian *et al.*, 2008b). In addition, during their long-distance evolution, many SIRs and ICMEs have merged into hybrid events. About 35% of SIRs and 37% of ICMEs occurred in hybrid events. The fraction was smaller during phase 3.

We were only able to sort 48% of the ICMEs into the three groups introduced in Section 3.2, based on the temporal P_{t} profile, because interactions between events added significant complexity to the simple ICME morphology and also because ICMEs weakened as they evolved. Among the classifiable ICMEs, the fractions in the three groups were, respectively, 27.6%, 44.8%, and 27.6%. These fractions had no clear solar-cycle dependence, perhaps partially owing to the poor statistics.

Table 2 Statistics of SIRs around 5.3 AU within ± 10° of ecliptic plane.

Phase #	Time interval	Quantity	Duration [days]	Width [AU]	P_{dynmax} [nPa]	P_{tmax} [pPa]	B_{max} [nT]	V_{mean} [km s^{-1}]	ΔV [km s^{-1}]	T_{min} [kK]	T_{max} [kK]	T_{mean} [kK]	R_T (T_{max}/T_{min})	R_D[a] (D_{before}/D_{after})
1	1997/291 –	Average	5.0 ± 0.2[b]	1.20 ± 0.07	0.53 ± 0.08	3.5 ± 0.6	2.2 ± 0.2	417 ± 15	73 ± 9	22 ± 2	161 ± 33	92 ± 17	7.0 ± 1.0	1.83 ± 0.77
	1998/331	Median	4.8	1.14	0.50	2.9	2.0	402	65	23	132	78	6.1	0.86
2	1992/65 –	Average	4.9 ± 0.5	1.39 ± 0.15	0.97 ± 0.15	8.6 ± 2.4	3.3 ± 0.5	497 ± 26	148 ± 30	42 ± 6	314 ± 61	178 ± 32	7.8 ± 1.2	1.04 ± 0.48
	261	Median	5.0	1.21	0.88	6.1	2.8	491	134	36	234	144	6.9	0.44
3	2003/360 –	Average	4.1 ± 0.2	1.12 ± 0.06	0.69 ± 0.08	5.1 ± 1.1	2.5 ± 0.2	481 ± 13	79 ± 10	40 ± 3	266 ± 44	153 ± 23	6.7 ± 0.7	0.66 ± 0.13
	2005/30	Median	4.3	1.16	0.60	3.2	2.1	472	66	35	218	127	6.4	0.47
Average			4.5 ± 0.2	1.19 ± 0.05	0.70 ± 0.06	5.3 ± 0.8	2.6 ± 0.2	466 ± 10	90 ± 9	36 ± 2	246 ± 29	141 ± 15	7.0 ± 0.5	1.06 ± 0.25
Median			4.5	1.16	0.60	3.5	2.2	448	68	31	197	114	6.3	0.47
Maximum			8.1	2.33	2.00	31.3	6.6	668	320	80	1355	710	21.0	11.78
Minimum			1.2	0.36	0.20	1.0	1.2	364	5	14	55	36	2.8	0.02

[a] R_D is the ratio of duration before stream interface to the duration after interface within a SIR.

[b] Average ± the probable error of the mean.

Table 3 Statistics of ICMEs around 5.3 AU within ± 10° of solar ecliptic plane.

Phase #	Time interval	Quantity	Duration [days]	Width [AU]	P_{dynmax} [nPa]	P_{tmax} [pPa]	B_{max} [nT]	V_{mean} [km s^{-1}]	$\lvert\Delta V\rvert$ [km s^{-1}]	T_{min} [kK]	T_{max} [kK]	T_{mean} [kK]	R_T ($T_{\mathrm{max}}/T_{\mathrm{min}}$)
1	1997/291 –	Average	3.7 ± 0.4	0.86 ± 0.09	0.30 ± 0.05	2.0 ± 0.3	1.7 ± 0.1	406 ± 10	55 ± 5	23 ± 1	104 ± 17	63 ± 9	3.7 ± 0.4
	1998/331	Median	3.0	0.72	0.20	1.3	1.4	389	47	21	77	52	3.7
2	1992/65 –	Average	3.2 ± 0.7	0.83 ± 0.18	0.63 ± 0.16	4.8 ± 1.7	2.4 ± 0.4	457 ± 19	70 ± 12	44 ± 13	147 ± 37	96 ± 24	4.5 ± 0.5
	261	Median	2.4	0.62	0.30	2.5	2.0	443	69	28	93	59	3.4
3	2003/360 –	Average	2.6 ± 0.4	0.71 ± 0.11	0.42 ± 0.08	3.1 ± 0.8	1.9 ± 0.3	481 ± 27	72 ± 17	42 ± 6	187 ± 64	114 ± 33	4.3 ± 1.1
	2005/30	Median	2.7	0.70	0.40	2.1	1.7	486	50	43	107	76	3.3
Average			3.4 ± 0.4	0.83 ± 0.10	0.41 ± 0.05	3.0 ± 0.7	1.9 ± 0.2	433 ± 13	62 ± 5	32 ± 4	131 ± 18	81 ± 15	4.2 ± 0.5
Median			3.0	0.70	0.30	1.8	1.6	419	50	25	85	55	3.4
Maximum			8.7	2.25	2.00	21.7	6.6	699	217	220	791	429	15.1
Minimum			0.2	0.05	0.03	0.4	0.7	341	19	12	35	25	1.5

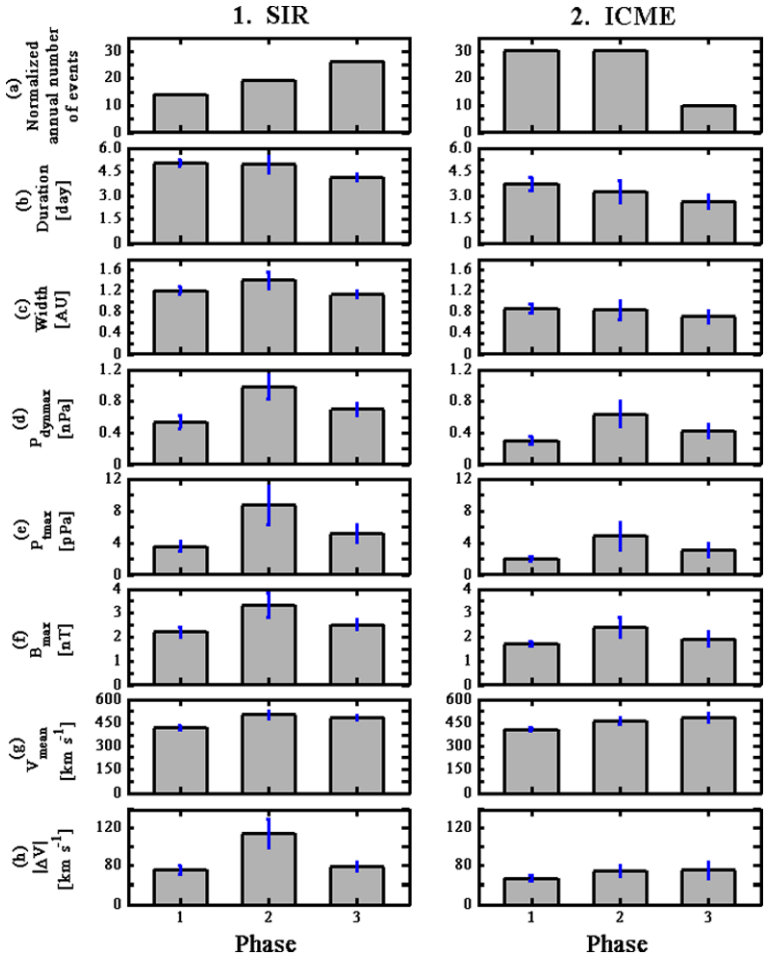

Figure 9 The solar-cycle-phase variations of the properties of SIRs and ICMEs. Phases are defined in Table 1 and Figure 2. From top to bottom are normalized annual number of events, duration, width, maximum of $P_{\rm dyn}$, maximum of $P_{\rm t}$, maximum field strength, mean solar-wind velocity, and absolute value of maximum velocity change. SIR and ICME parameters are shown on the same scale. The vertical line indicates the probable error of the mean.

Over the three phases, 91% of SIRs occurred with shocks (Table 1), significantly more than at and within 1 AU. Of the 91%, 47% were forward–reverse shock pairs, 41% were forward shocks only, and 12% were reverse shocks only. The dominance of forward shocks being associated with SIRs near the ecliptic plane is consistent with the in-ecliptic *Ulysses* observations of Gosling and Pizzo (1999). There are two explanations. First, because reverse shocks are formed at the trailing edge of SIRs (*i.e.*, usually in a fast stream with a low density and a higher temperature), the fast-mode magnetosonic speed is higher and it needs more compression to form a reverse shock (Jian *et al.*, 2006a). It is possible that some reverse shocks are still being formed at 5.3 AU. Second, even if both forward and reverse shocks driven by SIRs are well formed at 5.3 AU, the forward shocks propagate equatorward in both hemispheres whereas the reverse shocks propagate poleward (Gosling and Pizzo, 1999). The

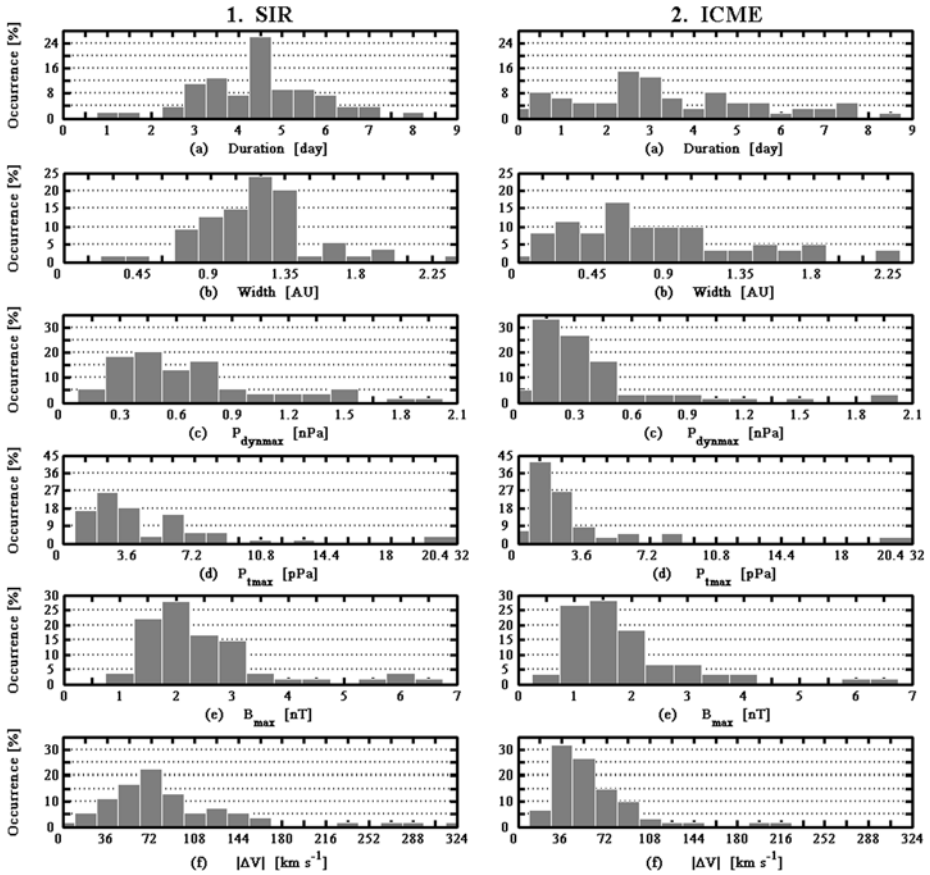

Figure 10 Histogram distributions of SIR and ICME properties during *Ulysses*' three aphelion passes. From top to bottom are duration, width, maximum of $P_{\rm dyn}$, maximum of $P_{\rm t}$, maximum magnetic field strength ($B_{\rm max}$), and absolute value of maximum velocity change ($|\Delta V|$). SIR and ICME parameters are shown on the same scale. The last bin of $P_{\rm tmax}$ is set to 20.4 – 32 pPa, because of its large variation range. Bins of other parameters are all set evenly.

probability of encountering a forward shock in the ecliptic plane is larger. To understand the relationship between shock properties and HCS location, a further detailed case study is needed.

About 58% of ICMEs drove shocks at 5.3 AU, similar to the rate at and within 1 AU; 94% of these shocks were forward shocks only. Only two ICMEs occurred with reverse shocks, which were caused by interaction with SIRs. Such an ICME – fast stream interaction region may lead to strong planetary magnetic effects, which are of great interest to the community (*e.g.*, Zhao, 1992; Cane and Richardson, 1997; Fenrich and Luhmann, 1998; Crooker, 2000).

The annual shock association rate did not change significantly with solar activity, either for SIRs or ICMEs (Table 1). Including all shocks, overall there were more forward shocks than reverse shocks near the ecliptic plane. So, in short, our study has extended the in-ecliptic-plane phase 2 observations by González-Esparza *et al.* (1996) and found that for-

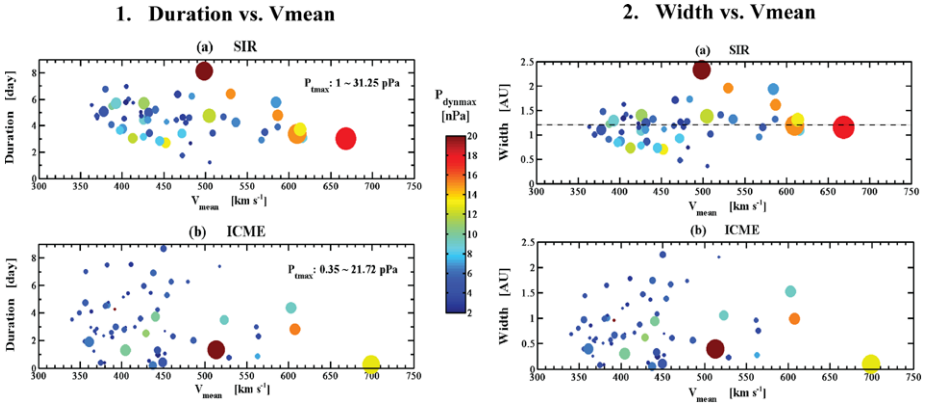

Figure 11 Duration and width versus mean velocity for (a) SIRs and (b) ICMEs, respectively. The radius of the circle for each event is proportional to P_{tmax}. The color shows P_{dynmax}. The SIR width, centered at about 1.2 AU, is marked by a dashed line, indicating that the SIR width is almost independent of V_{mean}.

ward shocks are also dominant in the in-ecliptic-plane solar wind during other solar cycle phases.

4.2. Duration and Width

On average, SIRs lasted longer than ICMEs at 5.3 AU. This trend was also true for each phase, shown in Figure 9(b). The median duration of SIRs was 4.5 days, whereas the median duration of ICMEs was 3.0 days. Over half of the SIRs had durations in a narrow range of 3 – 5 days, whereas the ICME durations were distributed more uniformly (Figure 10(a)). Notably in Figure 11, one SIR and one ICME lasted more than 8 days. The long-duration SIR was a hybrid event, with a flux rope embedded. The ICME lasting over 8 days contained multiple flux ropes, as in the case illustrated in Figure 6. Because it is hard to separate each individual structure, the whole event ended up having a long duration. In addition, the duration of an ICME also depends on the trajectory of its propagation with respect to the spacecraft. With the large Parker spiral angle at 5.3 AU, the ICME does not simply propagate radially out in the spacecraft frame and sometimes takes a long time to penetrate. Such long-duration events are uncommon. The stream interaction survey from 1 to 5 AU in González-Esparza and Smith (1996) using *Voyager* 1/2, *Ulysses* (1991 – 1992), and *Pioneer* 10/11 data and the online ICME list of Gosling and Reisefeld using *Ulysses* 1992 – 2002 observations (http://swoops.lanl.gov/cme_list.html) contain similar long-duration SIRs and ICMEs, although they did not pick out the same events as we did. Some of the long-duration SIRs might be caused by the merging of several shocks and small streams near the Sun. Alternatively, some of the long-duration ICMEs might be formed by the merging of a sequence of CMEs coming out at the same or adjacent active region on the Sun.

The location of the stream interface is important for SIR modeling. R_{D} denotes the ratio of the duration before the stream interface to the duration after the SI. R_{D} declined from phase 1 to 3, indicating a larger fraction of the duration was occupied by the trailing part from phase 1 to 3. The average and median values differ, because of some extremely large R_{D} values.

At 5.3 AU the Parker spiral angle is close to 90°. Based on the assumption that the stream interface follows the Parker spiral in the equatorial plane (Figure 1), the radial extent (line

AB) should be almost perpendicular to the stream interface within a SIR. Hence, the radial extent at 5.3 AU is of interest for the study of SIR radial evolution. From the product of duration and mean velocity (approximated by the mean of $V_{\rm max}$ and $V_{\rm min}$), we can estimate the radial extent of each event. To be consistent with our previous study, the radial extent is called "width". Width is also useful for describing ICMEs, since the ICMEs propagate roughly radially across the spacecraft.

Neither the SIR nor ICME width showed a strong solar-cycle dependence. The median width was 1.16 AU for SIRs and 0.70 AU for ICMEs. To be consistent for all groups of ICMEs, the ICME width includes the sheath region if there is one. Such a definition is meaningful in its own right based on the following three factors. First, the sheath region has been commonly assumed as the interplanetary counterpart of the bright front (Forsyth *et al.*, 2006), which is one part of the typical three-part CME structure (Hundhausen, 1988). Second, the compressed sheath regions with increased density and enhanced North – South magnetic-field component can greatly affect planetary magnetospheres (Crooker, 2000). Third, the sheath regions are often associated with the cosmic-ray Forbush decrease (*e.g.*, Burlaga, 1991). By taking into account the sheath region, we conclude that our ICME size is comparable with the MC size of Crooker *et al.* (2004) from the *Ulysses* 1990 to 2002 observations. About 70% of SIRs were 0.8- to 1.4-AU wide, whereas the widths of ICMEs were much more variable, as demonstrated in Figure 10(b) and Figure 11(2). Some ICMEs were smaller than 0.1 AU (Figure 11(2b)). Most such ICMEs occurred in hybrid events, and the ICME features only survived for a short while, such as the example in Figure 7. Another possibility is that the spacecraft only penetrated a small part of a larger ICME. In this scenario, the different groups of ICMEs may have different sizes. We will examine this correlation in future using our comprehensive survey.

4.3. Maximum Dynamic Pressure

The maximum dynamic pressure $P_{\rm dynmax}$ of SIRs had a median of 0.6 nPa, about five times of the median $P_{\rm dyn}$ for general solar wind (0.13 nPa, including the quiet time and disturbed time with SIRs and ICMEs, covering the *Ulysses* 3 aphelion passes), whereas the median $P_{\rm dynmax}$ of ICMEs was 0.3 nPa. So SIRs and ICMEs with large $P_{\rm dyn}$ could cause substantial changes of the location of the Jovian bow shock and magnetosphere. With a larger $P_{\rm dynmax}$ and a longer $P_{\rm dyn}$ compression, SIRs may in general have a more significant effect on the magnetopause location than ICMEs. $P_{\rm dynmax}$ was larger in phase 2, after the maximum of solar cycle 22, for both SIRs and ICMEs, suggesting a higher potential to compress Jovian magnetosphere post solar maximum.

In about 61% of SIRs at 5.3 AU, $P_{\rm dyn}$ maximized within 6 hours of the stream interface. Among the ICMEs with clear obstacle and/or sheath regions, 57% of ICMEs had maximum $P_{\rm dyn}$ in the magnetic obstacle. So the region near the stream interface or within a magnetic obstacle would be an interesting region to study the effect of solar-wind $P_{\rm dyn}$ on the Jovian magnetosphere.

Of the 60 ICMEs, 75% had $P_{\rm dynmax}$ smaller than 0.6 nPa, whereas the $P_{\rm dynmax}$ of SIRs was distributed more broadly than that of ICMEs (illustrated in Figure 10 and also by more colorful circles in the SIR panels of Figure 11). Both SIRs and ICMEs had a maximum $P_{\rm dynmax}$ of 2 nPa. In response to the highly variable solar wind $P_{\rm dyn}$, the shapes and locations of the Jovian magnetopause and bow shock would be also quite variable (Smith, Fillilius, and Wolfe, 1978; Smith *et al.*, 1981; Slavin *et al.*, 1985).

Joy *et al.* (2002) found a bimodal distribution of the observed Jovian magnetopause locations. As shown in Figure 10(c), the $P_{\rm dynmax}$ of SIRs and ICMEs had no bimodal distribution,

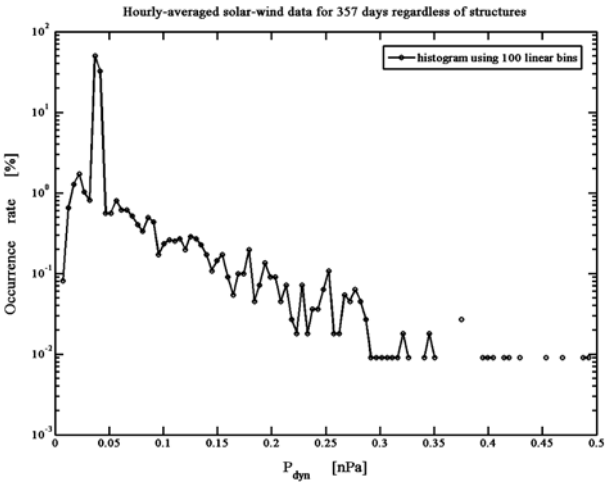

Figure 12 Histogram of all hourly averaged *Ulysses* solar-wind data at 5.3 AU for 357 days regardless of any structures, using 100 linear bins from 0 to 0.5 nPa. The data are confined within $\pm 6°$ in heliographic latitude (day 291 of 1997 – day 104 of 1998, day 360 of 2003 – day 172 of 2004), to match Jupiter's orbit range. The distribution has only one significant peak.

so we need to examine the general solar wind to find the source. To get enough SIRs and ICMEs to be statistically representative, we analyze the solar-wind structures within $\pm 10°$ ecliptic latitude. However, since we have enough solar-wind data, to best match the Jovian orbit range, we examined all the hourly averaged solar-wind data within $\pm 6°$ heliographic latitude. We find that the histogram of solar-wind $P_{\rm dyn}$ for these 357 days has one peak at about 0.039 nPa superimposed on a broader distribution, as illustrated in Figure 12. After several trials, we found that the sum of two log-normal distributions could fit the observation much better than one single log-normal distribution, as discussed in Joy *et al.* (2002). If we assume a solar-wind velocity of 450 km s^{-1}, the peak $P_{\rm dyn}$ corresponds to a $N_{\rm p}$ value of 0.1 cm^{-3}, less than a half of the general proton number density at 5.3 AU. So far, we do not know what caused the prominent $P_{\rm dyn}$ peak at such a low value. Because there is only one clearly defined peak in the distribution, it is not bimodal. Thus our observations of the solar wind near 5 AU do not provide the answer to the source of the bimodal magnetopause location of Jupiter other than to eliminate the solar wind as the source.

4.4. Maxima of Total Perpendicular Pressure and Magnetic Field

SIRs had a median total perpendicular pressure $P_{\rm tmax}$ of 3.5 pPa, almost twice that of ICMEs. Displayed in Figure 9(e), $P_{\rm tmax}$ in phase 2 was about twice that in phases 1 and 3, with larger variations, both for SIRs and ICMEs, although to different extents. This suggests that the interactions were stronger just post solar maximum. As illustrated in Figure 10(d), $P_{\rm tmax}$ of both SIRs and ICMEs was distributed mostly in the range of 1 – 7 pPa, with some events in long tails extending up to 32 pPa.

The median magnetic field $B_{\rm max}$ was 2.2 nT for SIRs and 1.6 nT for ICMEs. From the radial dependence of mean field intensity ($B_{\rm mean}$) of ICMEs in Liu, Richardson, and Belcher (2005) as well as Wang, Du, and Richardson (2005), we can estimate 0.7 nT as the $B_{\rm mean}$ of ICMEs at 5.3 AU. So the compression rate of magnetic field within ICMEs at Jovian orbit is about a factor of 2. As shown in Figure 9(f), the solar-cycle variation of $B_{\rm max}$ mimicked $P_{\rm dynmax}$ and $P_{\rm tmax}$ and was higher in phase 2 for both SIRs and ICMEs. $B_{\rm max}$ was slightly more variable for ICMEs than for SIRs. The similarity of $B_{\rm max}$ and $P_{\rm tmax}$ reflects the dominant contribution of B to $P_{\rm t}$.

4.5. Mean Velocity and Absolute Maximum Velocity Change

The mean velocity of each SIR and ICME was estimated by the average of $V_{\rm max}$ and $V_{\rm min}$ within the event. It varied moderately from phase to phase for both SIRs and ICMEs, as displayed in Figure 9(g). The median $V_{\rm mean}$ of SIRs was 448 km s^{-1}, about 30 km s^{-1} larger than that of ICMEs. The $V_{\rm mean}$ of ICMEs was distributed from 341 to 699 km s^{-1}, a little more widely than for SIRs (Figure 11).

Introduced in Section 3, the absolute maximum velocity change $|\Delta V|$ denotes the absolute value of the maximum velocity change within an event. The median $|\Delta V|$ was 68 km s^{-1} for SIRs and 50 km s^{-1} for ICMEs, both much smaller than in the inner heliosphere (Jian *et al.*, 2008b). Since $|\Delta V|$ is also the expansion velocity for ICMEs, the comparison suggests that the ICME expansion rate is less than the rate within 1 AU, in agreement with other studies based on other multiple spacecraft (*e.g.*, González-Esparza *et al.*, 1998; Liu, Richardson, and Belcher, 2005; Wang, Du, and Richardson, 2005). The $|\Delta V|$ values of SIRs changed significantly with solar activity, being largest in phase 2, whereas $|\Delta V|$ of ICMEs showed little solar-cycle dependence (Figure 9(h)). Additionally, $|\Delta V|$ of both SIRs and ICMEs was highly variable, particularly for SIRs (Figure 10(f)).

4.6. Proton Temperature

From Tables 2 and 3, we can see that $T_{\rm min}$, $T_{\rm max}$, $T_{\rm mean}$ (estimated by the average of $T_{\rm min}$ and $T_{\rm max}$), and $R_{\rm T}$ (defined as $T_{\rm max}/T_{\rm min}$) values of SIRs were larger than those of ICMEs. The median SIR $T_{\rm mean}$ was 114 kK, more than twice the median ICME $T_{\rm mean}$. If one considers the similar bulk velocities of SIRs and ICMEs, the difference in temperature is consistent with the fact that an ICME usually contains cooler plasma than the quiet solar wind for same bulk velocity (*e.g.*, Gosling, Pizzo, and Bame, 1973; Richardson and Cane, 1995), while the compression within a SIR can heat plasma.

From the median $R_{\rm T}$, we can see that the proton temperature usually varied by about a factor of 6 within a SIR and by only a factor of 3 within an ICME. The larger temperature variation within a SIR is likely related to the heating effect of the stream interaction. In future studies, the temperature variations of SIRs and ICMEs with heliocentric distance could tell us more about the solar-wind heating associated with these two large-scale structures.

4.7. Discussion

For almost all the properties listed in Tables 2 and 3, the average and median values of SIRs were larger than those of ICMEs. There were significant variations in the properties of both SIRs and ICMEs, even though they were all observed at nearly the same heliocentric distance around the ecliptic plane. In part, such variability suggests that the structures have different solar imprints or evolved in different ways. However, if these structures do have similar properties, the variability indicates that the observed properties may significantly depend on where the spacecraft have encountered the structures. Event study by multiple spacecraft, such as STEREO, ACE, and *Wind*, which are close by each other, may help address the second possibility.

Among the three phases, the normalized annual number of SIRs was largest in the declining phase, and the occurrence rate of ICMEs was higher close to solar maximum. SIR width, $P_{\rm dynmax}$, $P_{\rm tmax}$, $B_{\rm max}$, and $|\Delta V|$ were larger in phase 2 than in other phases, perhaps owing to the strong solar activity post solar maximum. ICME $P_{\rm dynmax}$, $P_{\rm tmax}$, and $B_{\rm max}$ were also larger in phase 2. Other properties did not show a clear solar-phase dependence.

From Figure 11(1), we can obtain the following rough correlations. SIRs and ICMEs with fast V_{mean} typically had relatively short durations. Higher V_{mean} was associated with larger P_{tmax} and P_{dynmax}, for both SIRs and ICMEs. Events with larger P_{tmax} were more likely to have stronger P_{dynmax}. ICMEs with larger P_{tmax} and P_{dynmax} typically had shorter durations. Using width instead of duration in Figure 11(2), we find that the SIR width was almost independent of V_{mean}, distributed around 1.2 AU, whereas the ICME width behaves very much like the duration and has a large variation.

After more than 17 years in space, *Ulysses* is likely to be decommissioned sometime in 2008, owing to telemetry and thermal problems. We do not expect *Ulysses* to accomplish its fourth aphelion passage in 2010. We hope future missions can provide the long-term observations at Jovian distance to improve our solar-cycle variations and statistics of SIRs and ICMEs at 5.3 AU.

5. Radial Evolution of SIRs and ICMEs from 0.72 to 5.3 AU

From 0.72 to 5.3 AU, the average annual occurrence rate of SIRs decreases from about 35 to 20 per year, probably because small and transient streams have merged as they evolve to 5.3 AU. Studies of some events using multipoint observations when *Ulysses* and other spacecraft (*e.g.*, *Wind* and ACE) are in radial alignment can help understand the formation of merged interaction regions (MIRs) (*e.g.*, Lazarus *et al.*, 1999). The average annual number of CIRs is around 14 – 20 at all distances; thus the CIR fraction increases with heliocentric distance. The shock association rate of SIRs increases greatly, from 3% to 91%, as they evolve from 0.72 to 5.3 AU. More forward – reverse shock pairs are formed at larger heliocentric distances. Besides the shock pairs, the forward shocks remain predominant.

The average annual ICME occurrence rate has no obvious radial variation, being around 20 events per year. The shock association rate of ICMEs changes slightly, increasing from 0.72 to 1 AU, then decreasing slightly beyond 1 AU. Since the occurrence rate of ICMEs strongly depends on solar activity, differences in solar activity level can cause large differences in the occurrence rate. Our 5.3-AU study did not have solar maximum data. It could skew the statistics somewhat as a function of heliocentric distance. We hope future observations at the Jupiter orbit can fill the solar maximum data gap and maybe during that time we can also correlate the solar-wind measurements with Jovian magnetospheric activity. In addition, ICMEs can become harder to distinguish as they evolve. It will be helpful to include unusual ion charge states and other composition signatures to identify ICMEs in future studies, because such signatures do not change much with ICME evolution.

From the orbit of Venus to Earth to Jupiter, the median width of SIRs (W_{SIR}), perpendicular to the stream interface in the equatorial plane, increases by a factor of more than 3, from 0.20 to 0.24 to 1.16 AU. As illustrated in Figure 13(1), W_{SIR} increases approximately linearly with heliocentric distance, as $W_{\mathrm{SIR}} = 0.21 \times R + 0.04$, where R is the heliocentric distance in AU, from 0.72 to 5.4 AU.

In contrast, across the 4.6-AU separation, the median width of ICMEs (W_{ICME}) increases from 0.27 to 0.70 AU. Assuming the median angular width of a CME is 40° at 15 R_{S} (Yashiro *et al.*, 2004; Gopalswamy, 2006), we estimate the width close to the Sun. Using a power-law fit to the three points within and at 1 AU, we find W_{ICME} increases with R approximately as $W_{\mathrm{ICME}} = 0.37 \times R^{0.85}$, where R is from 0.016 to 1 AU, as displayed in Figure 13(2). This is consistent with the theoretical conclusion by Chen (1996), as well as the observational results from Bothmer and Schwenn (1994) and Wang, Du, and Richardson (2005). However, if the ICME remains anchored to the Sun as it expands and if the magnetic

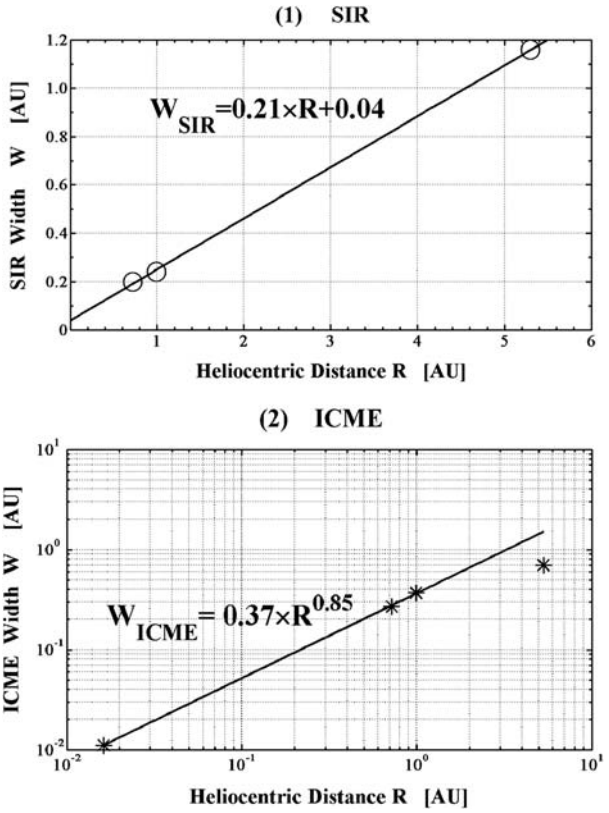

Figure 13 Variation of (1) SIR and (2) ICME width with heliocentric distance. The solid line in (1) is a linear fit for SIR width; the solid line in (2) is a power-law fit for ICME width from 0.016 to 1 AU. At 5.3 AU, the observed ICME width is about 0.6 AU smaller than the extrapolation from the power-law fit of the width within and at 1 AU, indicating ICME expansion weakens somewhere between 1 and 5.3 AU.

flux and helicity are constant, we expect the width of the flux rope to vary as R. However, the observed width at 5.3 AU is about 0.6 AU smaller than the extrapolation from our power-law fit, indicating that the ICME expansion significantly weakens somewhere from 1 to 5.3 AU. In short, the comparison of $W_{\rm SIR}$ and $W_{\rm ICME}$ indicates that SIRs expand faster than ICMEs with heliocentric distance.

$P_{\rm tmax}$ and $B_{\rm max}$ decrease with heliocentric distance, most strongly in ICMEs, next in the ambient solar wind, and least in SIRs. Thus the importance of SIRs in the solar wind becomes more significant at 5.3 AU. Within the 4.6-AU separation, the expansion velocity of ICMEs decreases from 115 to 50 km s^{-1}, and the fast magnetosonic Mach number (expansion speed over fast magnetosonic speed) decreases from 1.53 to 1.18, both again suggesting that the ICME expansion slows down remarkably, although it is still super-magnetosonic on average.

We note that to undertake this study of the variation with heliocentric distance, we have had to compare data obtained in different solar cycles. However, we do not believe the main results would be affected greatly by cycle-to-cycle differences in solar activity. Eventually, we hope to understand the radial evolution of SIRs and ICMEs by simultaneous multi-spacecraft observations at different heliocentric distances. The STEREO, ACE, *Wind*, *Venus Express*, *Ulysses*, and the proposed joint *Solar Sentinels* and *Solar Orbiter* missions would provide good opportunities to conduct such studies.

Acknowledgements This work has been jointly supported by the IGPP branch at Los Alamos National Lab (LANL) and by the NASA STEREO program through a grant administered by UCB. Work at Los Alamos

was performed under the auspices of the U.S. Department of Energy, with financial support from the NASA *Ulysses* program. We thank the LANL SWOOPS team (D.J. McComas), the magnetometer VHM/FGM team (A. Balogh), and NSSDC (J.F. Cooper) for making *Ulysses* data available.

References

Balogh, A., Beek, T.J., Forsyth, R.J., Hedgecock, P.C., Marquedant, R.J., Smith, E.J., Southwood, D.J., Tsurutani, B.T.: 1992, *Astron. Astrophys. Suppl.* **92**, 221.
Balogh, A., González-Esparza, J.A., Forsyth, R.J., Burton, M.E., Goldstein, B.E., Smith, E.J., Bame, S.J.: 1995, *Space Sci. Rev.* **72**, 171.
Balogh, A., Gosling, J.T., Jokipii, J.R., Kallenbach, R., Kunow, H. (eds.): 1999, *Space Sci. Rev.* **89**.
Bame, S.J., McComas, D.J., Barraclough, B.L., Phillips, J.L., Sofaly, K.J., Chavez, J.C., Goldstein, B.E., Sakurai, R.K.: 1992, *Astron. Astrophys. Suppl.* **92**, 237.
Belcher, J.W., Davis, L. Jr.: 1971, *J. Geophys. Res.* **76**, 3534.
Borrini, G., Gosling, J.T., Bame, S.J., Feldman, W.C.: 1982, *J. Geophys. Res.* **87**, 4365.
Bothmer, V., Schwenn, R.: 1994, *Space Sci. Rev.* **70**, 215.
Brueckner, G.E., Howard, R.A., Koomen, M.J., Korendyke, C.M., Michels, D.J., Moses, J.D., *et al.*: 1995, *Solar Phys.* **162**, 357.
Burlaga, L.F.: 1974, *J. Geophys. Res.* **79**, 3717.
Burlaga, L.F.: 1983, *J. Geophys. Res.* **88**, 6085.
Burlaga, L.F.: 1991, In: Schwenn, R., Marsch, E. (eds.) *Physics of the Inner Heliosphere 2*, Springer-Verlag, 1.
Burlaga, L.F., Sittler, E., Mariani, F., Schwenn, R.: 1981, *J. Geophys. Res.* **86**, 6673.
Burlaga, L.F., Klein, L.W., Lepping, R.P., Behannon, K.W.: 1984, *J. Geophys. Res.* **89**, 10659.
Cane, H.V., Richardson, I.G.: 1997, *J. Geophys. Res.* **102**, 17445.
Cane, H.V., Richardson, I.G.: 2003, *J. Geophys. Res.* **108**(A4), 1156.
Chen, J.: 1996, *J. Geophys. Res.* **101**, 27499.
Crooker, N.U.: 2000, *J. Atmos. Solar-Terr. Phys.* **62**, 1071.
Crooker, N.U., Horbury, T.S.: 2006, *Space Sci. Rev.* **123**, 93.
Crooker, N.U., Gosling, J.T., Kahler, S.W.: 2002, *J. Geophys. Res.* **107**(A2), 1028.
Crooker, N.U., Burton, M.E., Siscoe, G.L., Kahler, S.W., Gosling, J.T., Smith, E.J.: 1996, *J. Geophys. Res.* **101**(A11), 24331.
Crooker, N.U., Gosling, J.T., Bothmer, V., Forsyth, R.J., Gazis, P.R., Hewish, A., *et al.*: 1999, *Space Sci. Rev.* **89**, 179.
Crooker, N.U., Forsyth, R., Rees, A., Gosling, J.T., Kahler, S.W.: 2004, *J. Geophys. Res.* **109**, A06110.
de Kong, C.A., Steinberg, J.T., Gosling, J.T., Reisenfeld, D.B., Skoug, R.M., St. Cyr, O.C., Malayeri, M.L., Balogh, A., Rees, A., McComas, D.J.: 2005, *J. Geophys. Res.* **110**, A01102.
Du, D., Wang, C., Hu, Q.: 2007, *J. Geophys. Res.* **112**, A09101.
Fenrich, F.R., Luhmann, J.G.: 1998, *Geophys. Res. Lett.* **25**, 2999.
Forsyth, R.J., Bothmer, V., Cid, C., Crooker, N.U., Horbury, T.S., *et al.*: 2006, *Space Sci. Rev.* **123**, 383.
Ge, Y.S., Jian, L.K., Russell, C.T.: 2007, *Geophys. Res. Lett.* **34**, L23106.
González-Esparza, J.A., Smith, E.J.: 1996, *J. Geophys. Res.* **101**, 24359.
González-Esparza, J.A., Smith, E.J.: 1997, *J. Geophys. Res.* **102**, 9781.
González-Esparza, J.A., Balogh, A., Forsyth, R.J., Neugebauer, M., Smith, E.J., Phillips, J.L.: 1996, *J. Geophys. Res.* **101**, 17057.
González-Esparza, J.A., Neugebauer, M., Smith, E.J., Phillips, J.L.: 1998, *J. Geophys. Res.* **103**, 4767.
Gopalswamy, N.: 2006, *J. Astrophys. Astron.* **27**, 243.
Gopalswamy, N., Yashiro, S., Liu, Y., Michalek, G., Vourlidas, A., Kaiser, M.L., Howard, R.A.: 2006, *J. Geophys. Res.* **110**, A09 S15.
Gosling, J.T.: 1997, In: Crooker, N., Joselyn, J.A., Feynman, J. (eds.) *Coronal Mass Ejections*, *Geophys. Monograph* **99**, AGU, Washington, 9.
Gosling, J.T., Forsyth, R.J.: 2001, *Space Sci. Rev* **97**, 87.
Gosling, J.T., Pizzo, V.J.: 1999, *Space Sci. Rev* **89**, 21.
Gosling, J.T., Pizzo, V., Bame, S.J.: 1973, *J. Geophys. Res.* **78**, 2001.
Gosling, J.T., Birn, J., Hesse, M.: 1995, *Geophys. Res. Lett.* **22**, 869.
Gosling, J.T., Asbridge, J.R., Bame, S.J., Feldman, W.C.: 1978, *J. Geophys. Res.* **83**, 1401.
Gosling, J.T., McComas, D.J., Phillips, J.L., Feldman, W.C.: 1991, *J. Geophys. Res.* **96**, 7831.
Hundhausen, A.J.: 1988, In: Pizzo, V.J., Holzer, T.E., Sime, D.G. (eds.) *Proceedings of the Sixth International Solar Wind Conference, Rep. TN-306*, NCAR, Boulder, 181.

Hundhausen, A.J., Gosling, J.T.: 1976, *J. Geophys. Res.* **81**, 1436.
Intriligator, D.S., Siscoe, G.L., Wibberenz, G., Kunow, H., Gosling, J.T.: 1995, *Geophys. Res. Lett.* **22**, 1173.
Jian, L., Russell, C.T., Gosling, J.T., Luhmann, J.G.: 2005a, In: Fleck, B., Zurbuchen, T.H., Lacoste, H. (eds.) *Connecting Sun and Heliosphere*, *Proc. Solar Wind 11/SOHO 16* **SP-592**, ESA, Noordwijk, 491.
Jian, L., Russell, C.T., Gosling, J.T., Luhmann, J.G.: 2005b, In: Fleck, B., Zurbuchen, T.H., Lacoste, H. (eds.) *Connecting Sun and Heliosphere*, *Proc. Solar Wind 11/SOHO 16* **SP-592**, ESA, Noordwijk, 731.
Jian, L., Russell, C.T., Luhmann, J.G., Skoug, R.M.: 2006a, *Solar Phys.* **239**, 337.
Jian, L., Russell, C.T., Luhmann, J.G., Skoug, R.M.: 2006b, *Solar Phys.* **239**, 393.
Jian, L.K., Russell, C.T., Luhmann, J.G., Skoug, R.M.: 2008a, *Adv. Space Res.* **41**, 259.
Jian, L.K., Russell, C.T., Luhmann, J.G., Skoug, R.M., Steinberg, J.T.: 2008b, *Solar Phys.* **249**, 85.
Joy, S.P., Kivelson, M.G., Walker, R.J., Khurana, K.K., Russell, C.T., Ogino, T.: 2002, *J. Geophys. Res* **107**(A10), 1309.
Klein, L.W., Burlaga, L.F.: 1982, *J. Geophys. Res* **87**, 613.
Lazarus, A.J., Richardson, J.D., Decker, R.B., McDonald, F.B.: 1999, *Space Sci. Rev* **89**, 53.
Lepping, R.P., Jones, J.A., Burlaga, L.F.: 1990, *J. Geophys. Res* **95**, 11957.
Liu, Y., Richardson, J.D., Belcher, J.W.: 2005, *Planet. Space Sci.* **53**, 3.
Luhmann, J.G., Li, Y., Arge, C.N., Gazis, P.R., Ulrich, R.: 2002, *J. Geophys. Res* **107**, 1154.
Manchester IV, W.B., Zurbuchen, T.H.: 2007, *J. Geophys. Res.* **112**, A07103.
Marubashi, K.: 1997, In: Crooker, N., Joselyn, J.A., Feynman, J. (eds.) *Coronal Mass Ejections*, *Geophys. Monograph* **99**, AGU, Washington, 147.
Murdin, P.: 2000, In: P. Murdin (ed.) *Encyclopedia of Astronomy and Astrophysics*, Article **4331**.
Neugebauer, M., Goldstein, R.: 1997, In: Crooker, N., Joselyn, J.A., Feynman, J. (eds.) *Coronal Mass Ejections*, *Geophys. Monograph* **99**, AGU, Washington, 245.
Osherovich, V., Burlaga, L.F.: 1997, In: Crooker, N., Joselyn, J.A., Feynman, J. (eds.) *Coronal Mass Ejections*, *Geophys. Monograph* **99**, AGU, Washington, 157.
Rees, A., Forsyth, R.J.: 2004, *Geophys. Res. Lett.* **31**, L06804.
Richardson, I.G., Cane, H.V.: 1995, *J. Geophys. Res.* **100**, 23397.
Riley, P., Gosling, J.T.: 2007, *J. Geophys. Res.* **112**, A07102.
Riley, P., Schatzman, C., Cane, H.V., Richardson, I.G., Gopalswamy, N.: 2006, *Astrophys. J.* **647**, 648.
Russell, C.T., Shinde, A.A.: 2005, *Solar Phys* **229**, 323.
Russell, C.T., Shinde, A.A., Jian, L.K.: 2005, *Adv. Space Res.* **35**, 2178.
Schwenn, R.: 1990, In: Schwenn, R., Marsch, E. (eds.) *Physics of the Inner Heliosphere 1*, Springer-Verlag, 99.
Shodhan, S., Crooker, N.U., Kahler, S.W., Fitzenreiter, R.J., Larson, D.E., Lepping, R.P., Siscoe, G.L., Gosling, J.T.: 2000, *J. Geophys. Res.* **105**, 27261.
Siscoe, G., Intriligator, D.: 1993, *Geophys. Res. Lett.* **20**(20), 2267.
Slavin, J.A., Smith, E.J., Spreiter, J.R., Stahara, S.S.: 1985, *J. Geophys. Res.* **90**, 6275.
Smith, E.J., Wolfe, J.H.: 1976, *J. Geophys. Res.* **3**, 137.
Smith, E.J., Fillilius, R.W., Wolfe, J.H.: 1978, *J. Geophys. Res.* **83**, 4733.
Smith, Z.K., Dryer, M., Fillius, R.W., Smith, E.J., Wolfe, J.H.: 1981, *J. Geophys. Res.* **86**, 6773.
Southwood, D.J., Kivelson, M.G.: 2001, *J. Geophys. Res.* **106**, 6123.
Vasquez, B.J., Farrugia, C.J., Markovskii, S.A., Hollweg, J.V., Richardson, I.G., Ogilvie, K.W., Lepping, R.P., Lin, R.P., Larson, D.: 2001, *J. Geophys. Res.* **106**, 29283.
Wang, C., Du, D., Richardson, J.D.: 2005, *J. Geophys. Res.* **110**, A10107.
Wenzel, K.-P., Marsden, R.G., Page, D.E., Smith, E.J.: 1992, *Astron. Astrophys. Suppl.* **92**, 207.
Whang, Y.C., Burlaga, L.F., Ness, N.F., Smith, C.W.: 2001, *Solar Phys* **204**, 255.
Wimmer-Schweingruber, R.F., Crooker, N.U., Balogh, A., Bothmer, V., Forsyth, R.J., Gazis, P., *et al.*: 2006, *Space Sci. Rev.* **123**, 177.
Yashiro, S., Gopalswamy, N., Michalek, G., St. Cyr, O.C., Plunkett, S.P., Rich, N.B., Howard, R.A.: 2004, *J. Geophys. Res.* **109**, A07105.
Zhao, X.P.: 1992, *J. Geophys. Res.* **97**, 15051.
Zurbuchen, T.H., Richardson, I.G.: 2006, *Space Sci. Rev.* **123**, 31.